Shear Strength of Granular Soil Under Saturated and Unsaturated Conditions

Gregor Idinger and Wei Wu

Abstract The shear strength of soils depends on various factors such as the stress level, soil density, and degree of saturation. Capillary forces in unsaturated soils feature an increased strength against shear loading, and influence stress, deformation, and flow phenomena. Thus it is crucial to incorporate the bonding effect of unsaturated soils to numerical models addressing the behaviour of unsaturated soils. The presented experimental campaign of triaxial compression tests aims to investigate the effect of capillarity on the mechanical behaviour of granular soil. The experimental programme consists of consolidated-drained tests on saturated soils and equivalent constant suction tests on unsaturated soils with matric suction of 10 kPa. The results of the experimental campaign reflect the higher resistance of unsaturated soils against shear loading manifested by an additional apparent cohesion term and by suction-induced hardening.

1 Introduction

Soil water plays a key role for the stability of geotechnical structures. While positive pore water pressures have negative influence on the soil strength, negative pore pressures in partially saturated soils provide additional strength due to "bonding" effects of capillary forces. Classical theories of limit state soil mechanics implicitly assume that soils are either dry or saturated. However, soil near the ground surface is commonly in the unsaturated state in between these two extreme conditions. Thus,

G. Idinger (✉) · W. Wu
Institute of Geotechnical Engineering, University of Natural Resources and Life Sciences, Feistmantelstrasse 4, 1180 Vienna, Austria
e-mail: gregor.idinger@boku.ac.at

W. Wu
e-mail: wei.wu@boku.ac.at

W. Wu (ed.), *Recent Advances in Geotechnical Research*,
Springer Series in Geomechanics and Geoengineering,
https://doi.org/10.1007/978-3-319-89671-7_7

for many geotechnical applications the unsaturated condition of soils influences the performance of engineering structures.

Soils are heterogeneous geomaterials composed of the solid soil skeleton and the void space. Voids are filled with liquid and gaseous phases. Thereof, unsaturated soils are idealised by a three-phase model, with solids, water, and air. The soil skeleton consists of particles with solid density ρ_s, and its volumetric fraction is defined by the ratio of volume of void space per volume of solid fraction as the void ratio $e = V_v / V_s$. The void space occupied by the pore water V_w is indicated by the degree of saturation $S_r = V_w / V_v$. Water molecules of the air-water interface are attracted towards the liquid phase causing an unbalanced force. The generated surface tension T_s achieves equilibrium conditions along the contractile skin. This tensile force interacts with the soil particles and thereof controls the mechanical behaviour of the soil skeleton. In the capillary model the radius of curvature of the water-air interface is inversely proportional to the difference between air pressure u_a and water pressure u_w within the soil. The difference in pressure is called matric suction $s = u_a - u_w$. For multiphase porous media such as soils it is crucial to address those effects in constitutive models formulated for unsaturated soils.

The objective of the presented experimental campaign is to describe and quantify the coupled shear and volumetric behaviour of saturated and unsaturated specimen of granular soil.

2 Material and Methods

The experimental investigation is conducted on granular soil. The coupled shear and volumetric behaviour is determined experimentally with the double-cell triaxial apparatus on infinite small homogeneous soil specimens for both saturated and unsaturated conditions. The triaxial testing programme consists of consolidated-drained tests on saturated soils and equivalent constant suction tests on unsaturated soils.

2.1 Soil Material

The soil is classified as well-graded medium-fine sand with a minor fraction of silt (mfSa, si′). Figure 2 presents the grain size distribution curve. The mean diameter is $d_{50} = 0.23$ mm, the coefficient of uniformity $C_u = 13.6$ and the coefficient of curvature $C_c = 3.6$. The scanning-electron-microscope image of Fig. 1 visualizes the sub-angular shape of sand particles. The particle density of the medium-fine sand is determined with $\rho_s = 2.67$ g/cm^3, quartz sand is the main component. The minimum and maximum void ratio are defined with $e_{min} = 0.45$ and $e_{max} = 1.09$, respectively. Soil specimens are compacted to medium dense and very dense states, as listed in the triaxial testing programme of Table 1.

2.2 Double Cell Triaxial Apparatus

The concept of the double-cell triaxial apparatus introduced by Simon J. Wheeler in 1986 enables the measurement of volumetric strain of unsaturated soil specimen [6]. The axis translation technique is adopted to control matric suction inside the specimen by imposing a positive air pressure u_a and keeping the difference in global pressure $(u_a - u_w)$ unchanged.

The employed double-cell triaxial apparatus manufactured by *Wille Geotechnik* is illustrated in Fig. 3. The major principal stress σ_1 in axial direction is measured by the submerged load cell, the axial displacement is measured by the LVDT mounted on top of the triaxial cell. The pore air pressure u_a is injected through the porous stone on top of the specimen. The pore water pressure u_w is controlled through the lower ceramic disc with high air-entry-value at the bottom of the specimen, and is measured by the pressure transducer connected via the lower ceramic disc. The confining pressure σ_3 is provided and regulated by an automatic displacement-controlled hydraulic pressure system. The global volumetric strain ε_V is inferred from the ram displacement of the automatic pressure system for the inner cell to preserve constant confining pressure.

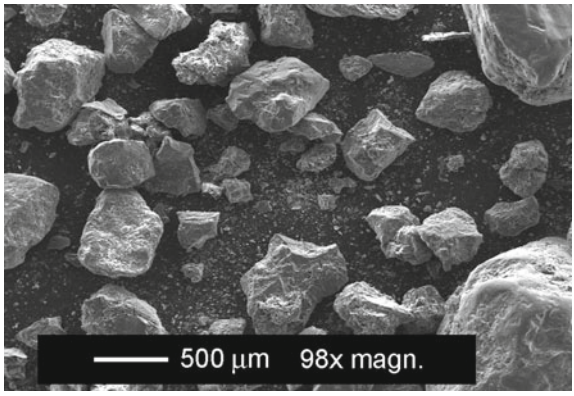

Fig. 1 Scanning electron microscope image of the granular soil

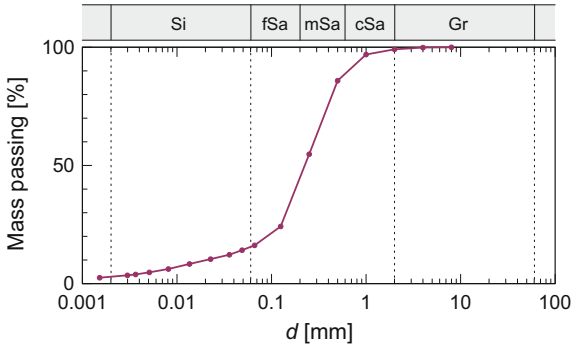

Fig. 2 Grain size distribution curve of the granular soil. Gr: 0.8%, Sa: 82.9%, Si: 13.4%, Cl: 2.8%

Table 1 Triaxial test programme with initial and failure conditions. Encoding of test identity: S - saturated, U - unsaturated; M - medium dense, D - very dense

Test	σ_3 (kPa)	e (–)	s (kPa)	w_0 (%)	w_f (%)	$S_{r,f}$ (%)	m (g)	p'_p (kPa)	q_p (kPa)	E (MPa)
SM	50	0.73	0.0	15.1	22.3*	81.2*	2958	73.2	93.1	10.0
	100	0.73	0.0	15.1	23.8*	86.6*	2964	170.1	220.1	11.5
	200	0.73	0.0	15.1	22.0*	81.3*	2969	343.5	438.7	14.6
UM	50	0.75	9.8	15.1	10.5	37.6	2931	79.2	110.9	14.5
	100	0.73	9.7	15.1	10.5	38.8	2968	169.8	230.5	16.0
	200	0.73	9.7	15.1	11.2	40.8	2961	342.1	450.6	18.2
SD	50	0.51	0.0	16.6	19.0	99.8	3426	121.9	218.4	30.7
	100	0.51	0.0	16.6	18.7	96.6	3448	233.3	404.2	57.3
	200	0.52	0.0	16.6	18.1	93.5	3418	431.6	699.4	68.0
UD	50	0.50	9.1	15.1	11.3	60.4	3409	118.7	224.1	30.0
	100	0.51	7.3	15.1	11.7	60.5	3385	233.8	415.8	49.0
	200	0.51	9.3	15.1	11.0	57.8	3396	437.6	730.5	69.6

*Drainage during unloading resulted in decrease of w_f and $S_{r,f}$

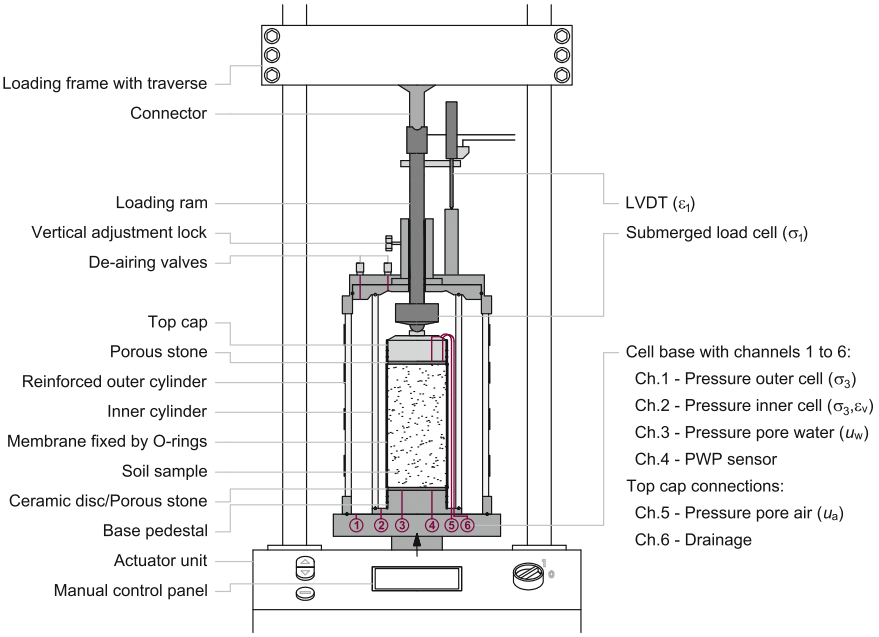

Fig. 3 Schematic drawing of the triaxial apparatus equipped with double cell configuration

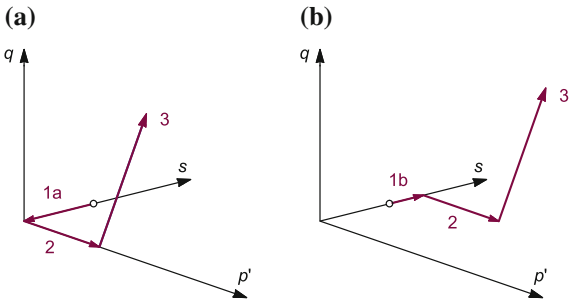

Fig. 4 Stress paths in the p'–q–s space for **a** saturated and **b** unsaturated triaxial compression tests, with 1a - initial saturation, 1b - setting of matric suction, 2 - consolidation, and 3 - drained axial compression

2.3 Testing Procedure

The triaxial testing programme consists of consolidated–drained tests for saturated specimen and equivalent constant suction tests for unsaturated specimen. The testing programme is summarized in Table 1. The stress paths are sketched in the p'–q–s space diagram of Fig. 4. Saturated soil specimen are initially saturated along path 1a with a back-pressure of 300 kPa. Unsaturated soil specimen are set to the desired matric suction along path 1b by applying the axis-translation technique. Soil specimens are of cylindrical shape with 100 mm in diameter and 200 mm in height. The soil is mixed at the optimum water content of $w_{opt} = 15.1\%$ and compacted by the moist-tamping technique in eight layers.

Four sets of triaxial tests are carried out: for medium dense $e = 0.74$ and very dense $e = 0.51$ compaction states under both saturated and unsaturated condition. The matric suction in the unsaturated tests is $s = 10$ kPa. This value corresponds to the intersection of the transition and residual zone of the SWCC [3]. Each set of tests consists of three individual tests isotropically consolidated to 50, 100, and 200 kPa. After reaching constant conditions, axial compression is applied at the strain rate of 0.02 mm/min.

3 Results and Interpretation

The axisymmetric confining pressure of the triaxial cell ($\sigma_2 = \sigma_3$) reduces the stress invariants mean effective stress p' and deviatoric stress q to

$$p' = \left(\sigma_1' + 2\sigma_3'\right)/3 \tag{1}$$

$$q = \sigma_1' - \sigma_3' \tag{2}$$

The Bishop effective stress definition for unsaturated soils [1] describes multiphase and multi-stress geomaterials by a mechanically equivalent single phase and stress state continuum on a macroscopic scale, written in the notation of

$$\sigma' = \sigma - u_a + \chi(u_a - u_w) \tag{3}$$

where σ' is the effective stress, σ the total external stress, u_a the pore air pressure, u_w the pore water pressure, and χ is Bishop's effective stress parameter. Bishop's parameter χ is related to a volumetric function of the fluid phase to define the influence of the negative pore water pressure, and varies from 0 for the dry state to 1 for the saturated state. With the simple assumption of $\chi = S_r$, proposed by Schrefler [5], Eq. 3 can be reformulated as

$$\sigma' = \sigma - u_a + S_r(u_a - u_w) \tag{4}$$

Under saturated conditions ($S_r = 1$, $u_a = 0$) Eq. 4 reduces to Terzaghi's effective stress formulation

$$\sigma'_{sat} = \sigma - u_w \tag{5}$$

3.1 Stress–Strain and Volumetric Behaviour

In Figs. 5 and 6 the deviatoric stress q and volumetric strain ε_V are plotted over the axial strain ε_1. At unsaturated conditions a noticeable increase in peak strength is reached at lower axial compression rates throughout all tests ("suction-induced hardening"). The elastic moduli E listed in Table 1 are inferred from the secants intersecting the stress–strain curve at 0.5 of the peak deviatoric stresses q_p. Resulting E-moduli lie in the range of 10–18 MPa for the medium dense, and 30–70 MPa for the very dense soils. For the medium dense soil the matric suction of $s = 10$ kPa results in an increase of E by about 60%. For the very dense soil E remains in the range of the saturated tests.

Tests on medium dense specimens show an asymptotic convergence towards maximum deviatoric stresses under both saturated and unsaturated conditions (Fig. 5). The peak deviatoric stress of the unsaturated soil increased by about 2–5%. The unsaturated specimen consolidated to $\sigma_3 = 50$ kPa records an increase in peak strength of 19%. The volume of saturated medium dense specimens decreases with increasing axial strain (Fig. 5a). The compression rate increases with increasing consolidation pressure. The unsaturated medium dense soil specimens experience reduced contraction upon loading. The medium dense soil consolidated at $\sigma_3 = 50$ kPa transforms from contractive behaviour in the saturated state to dilative behaviour in the unsaturated state.

Stress–strain curves for the very dense specimen in Fig. 6 reach peak stresses at axial compression of $3.4\% < \varepsilon_1 < 4.8\%$, followed by strain-softening in the plastic regime under both saturated and unsaturated conditions. The peak strength of the unsaturated very dense specimen is reached at shorter axial compression in the range of $2.7\% < \varepsilon_1 < 4.2\%$. Similar to the medium dense compaction state, the peak strengths increase by about 2–5%. Experiments on saturated very dense specimens reveal strong dilative response after short initial compression phases of $\varepsilon_1 < 1\%$

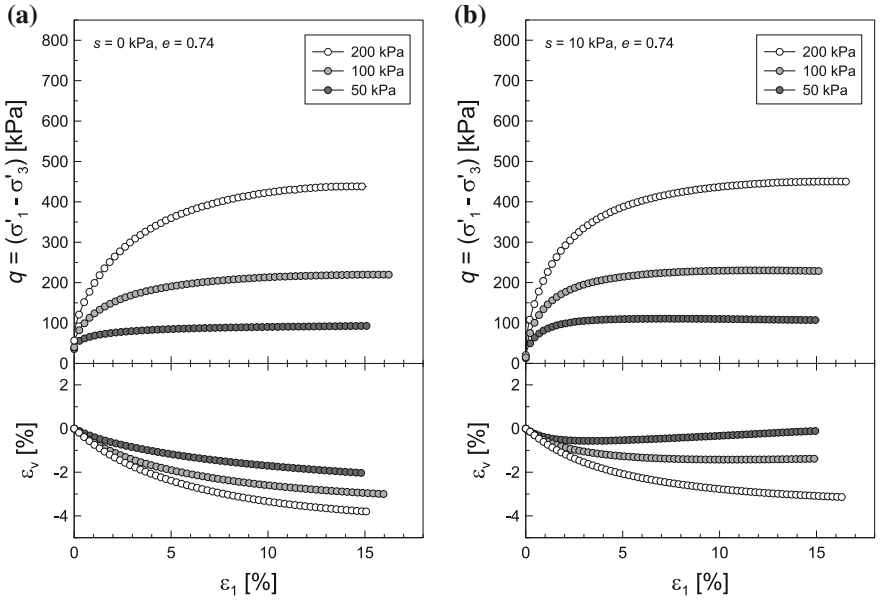

Fig. 5 Deviatoric stress and volumetric strain plotted over axial strain for the medium dense soil, under **a** saturated and **b** unsaturated conditions

(Fig. 6a). The volumetric response changes from contractive to dilative behaviour just before reaching peak stresses around axial compressions of $1\% < \varepsilon_1 < 3\%$. Smaller confining pressures result in larger dilatancy. The unsaturated soil state enhances the dilative response. The dilative rates $\dot{\varepsilon}_V$ decrease when reaching axial compressions between $5\% < \varepsilon_1 < 10\%$. The inflection points correspond with the softening regime, higher consolidation pressures result in inflection points at higher axial compressions ε_V. The shapes of the sheared soil specimen can be described by barrelling and shear failure along one distinct shear band.

Figure 7 presents the residual states of all conducted triaxial tests, resulting in a good fit for a unique critical state line for the saturated and unsaturated tests. The mean effective stress concept eliminates the influence of matric suction on the CSL [4]. The resulting critical state line has a grade coefficient $M = 1.385$ and coefficient of determination of $R^2 = 0.996$. The graphs of Fig. 6 show small decrease at residual conditions, thus corresponding points in Fig. 7 will converge towards the established critical state line.

3.2 Shear Strength

Figure 8 illustrates the stress paths and Mohr circles of the peak stress conditions in the σ'_m–τ plane, with

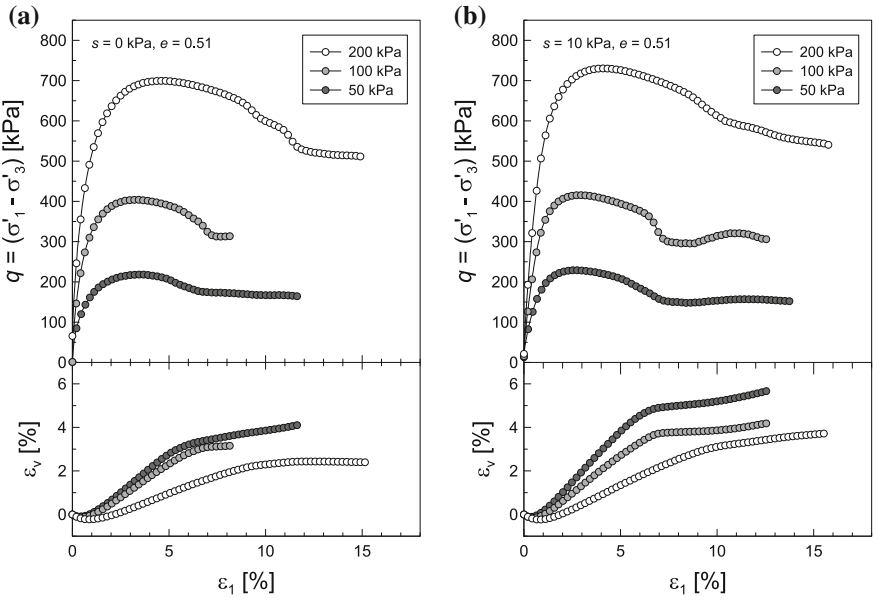

Fig. 6 Deviatoric stress and volumetric strain plotted over axial strain for the very dense soil, under **a** saturated and **b** unsaturated conditions

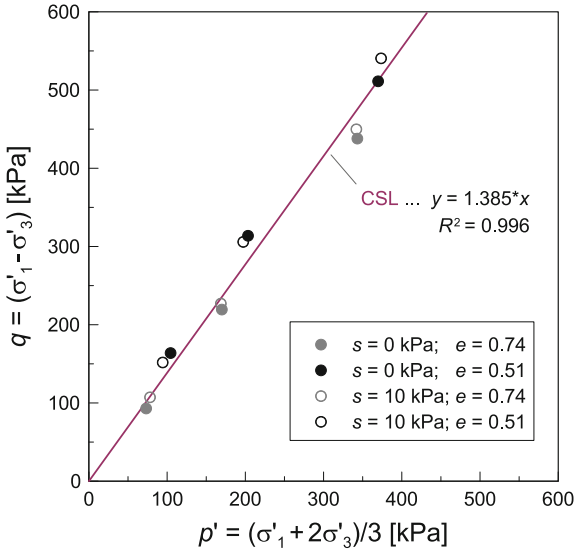

Fig. 7 Estimated critical state line (CSL) based on Bishop's effective stress definition

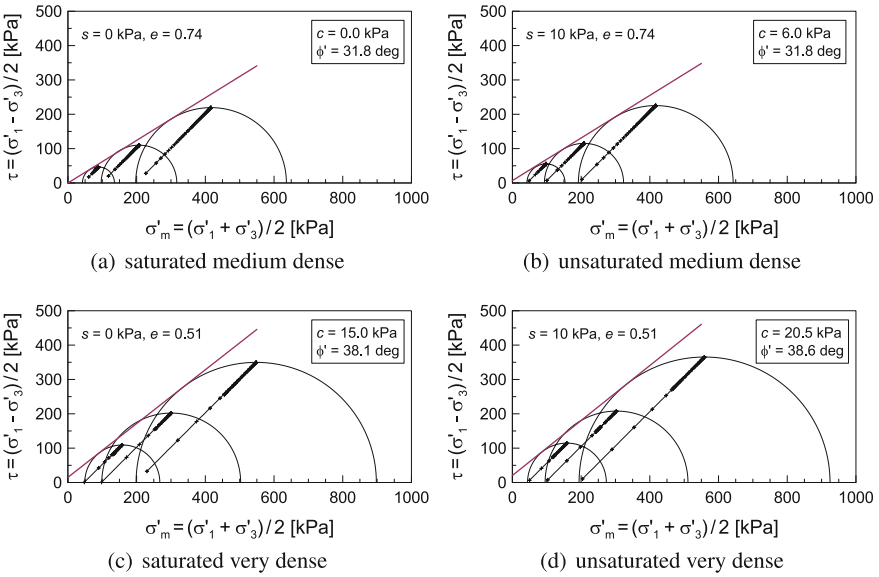

(a) saturated medium dense (b) unsaturated medium dense

(c) saturated very dense (d) unsaturated very dense

Fig. 8 Failure surface, Mohr circles for peak stresses, and stress paths of drained triaxial shear tests, with (**a**) and (**c**) saturated tests, (**b**) and (**d**) unsaturated tests with $s = 10\,\text{kPa}$

Table 2 Shear parameters obtained from drained triaxial shear tests under saturated and unsaturated conditions with $s = 10\,\text{kPa}$ for the peak and residual strength

	$e = 0.74$		$e = 0.51$			
	ϕ' (deg)	c' (kPa)	ϕ' (deg)	c' (kPa)	ϕ'_r (deg)	c'_r (kPa)
s = 0 kPa	31.8	0.0	38.1	15.0	33.0	0.0
s = 10 kPa	31.8	6.0	38.6	20.5	35.0	0.0

$$\sigma'_m = \left(\sigma'_1 + \sigma'_3\right) / 2 \tag{6}$$

$$\tau = \left(\sigma'_1 - \sigma'_3\right) / 2 \tag{7}$$

with σ'_m as the mean effective stress in the 2-dimensional stress space, and τ as the shear stress. The stress paths in Fig. 8 are represented by 1:1 slopes, starting at the confining pressures of 50, 100, and 200 kPa. The Mohr circles for the peak stresses indicate the stress state of failure condition. Mohr-Coulomb failure envelopes are drawn as tangential lines to the three Mohr circles of different confining pressure. The linear failure criteria show good fits for all performed test sets.

The Mohr-Coulomb shear parameters cohesion c' and friction angle ϕ' are summarized in Table 2. The examined saturated granular soil can be addressed as non-cohesive material in the medium dense compaction state, but exhibits an apparent cohesion of 15 kPa in the very dense state. The friction angle ϕ' of 31.8° for the

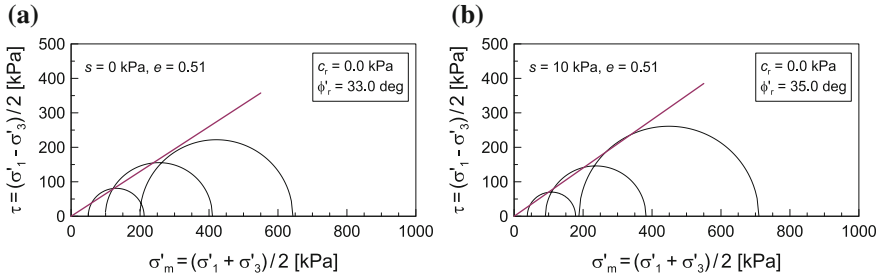

Fig. 9 Failure surface and Mohr circles for residual stresses of drained triaxial shear tests, with **a** saturated, and **b** unsaturated tests

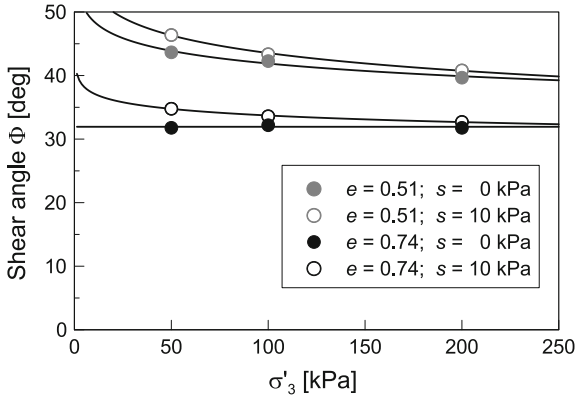

Fig. 10 Shear angle Φ as function of confining pressure σ_3

medium dense and 38.1° for the very dense compaction state is not effected by the applied matric suction of $s = 10$ kPa, whereas the cohesion term increases from $c' = 0.0$ to 6.0 kPa for the medium dense and from $c' = 15.0$ to 20.5 kPa for the very dense compaction state. The additional cohesion term c'' is in the order of 6 kPa for both the medium dense and very dense configuration. The soil parameter ϕ^b [2] is close to or significantly smaller than ϕ' for the medium dense and very dense compaction state, respectively. It is noted that ϕ^b is not constant and typically decreases with higher matric suction.

The residual strength for the very dense soil is illustrated in Fig. 9. With the cohesion set equal to zero the friction angle ϕ'_r reduces to 33° and 35° for the saturated and unsaturated condition, respectively.

Figure 10 plots the shear angle Φ as function of the confining pressure σ_3. A decrease of Φ with higher σ_3 is documented for the very dense soil and the unsaturated medium dense soil, whereas Φ of the saturated medium dense soil is unaffected by the confining pressure. The unsaturated soil state results in higher shear angles. The highest increase of shear angles is observed for the lowest confining pressure of 50 kPa.

4 Conclusions

In this paper, the significant contribution of capillarity to the mechanical behaviour and shear strength of the unsaturated granular soil under shear loading has been shown in the experimental investigation. The unsaturated soils with matric suction of $s = 10$ kPa show increase in peak stress at lower axial compression for both medium dense and very dense compaction states, a behaviour known as "suction-induced hardening". The applied matric suction reduces the contractive response upon loading, and can even result in dilative response of the granular soil. The increase in shear strength of the granular soil is expressed by an additional term of apparent cohesion. The applied matric suction increases the cohesion term by about 6 kPa, whereas the friction angle is not significantly affected by the unsaturated state under the examined condition. The additional strength from capillarity is most pronounced for the lowest investigated confining pressure.

Acknowledgements The support of the Otto Pregl Stiftung is greatly appreciated.

References

1. Bishop, A.W.: The principle of effective stress. Tecnisk Ukeblad **39**, 859–863 (1959)
2. Fredlund, D.G., Morgenstern, N.R., Widger, R.A.: The shear strength of unsaturated soils. Can. Geotech. J. **15**, 313–321 (1978)
3. Idinger, G.: Experimental study of failure initiation in partially saturated slopes. Ph.D. thesis, Universität für Bodenkultur, Wien (2016)
4. Nuth, M., Laloui, L.: Effective stress concept in unsaturated soils: clarification and validation of a unified framework. Int. J. Numer. Anal. Meth. Geomech. **32**(7), 771–801 (2008)
5. Schrefler, B.A.: The finite element method in soil consolidation (with applications to surface subsidence). Ph.D. thesis, University College of Swansea (1984)
6. Wheeler, S.J.: The stress-strain behavior of soils containing gas bubbles. Ph.D. thesis, The University of Oxford (1986)